Deactivation behavior of Pd/C and Pt/C catalysts in the gas-phase hydrodechlorination of chloromethanes: Structure–reactivity relationship

M. Martin-Martinez[a], A. Álvarez-Montero[a], L.M. Gómez-Sainero[a,*], R.T.Baker[b],
J. Palomar[a], S. Omar[a], S. Eser[c], J.J. Rodriguez[a]

[a] Sección de Ingeniería Química, Facultad de Ciencias, Universidad Autónoma de Madrid, Cantoblanco, 28049 Madrid, Spain
[b] School of Chemistry, University of St Andrews, North Haugh, St Andrews, Fife KY16 9ST, United Kingdom
[c] John and Willie Leone Family Department of Energy and Mineral Engineering and EMS Energy Institute, The Pennsylvania State University,
114A Hosler Building, University Park, PA 16802, United States

A B S T R A C T

This study analyzes the influence of chemical and physical properties of Pd/C and Pt/C hydrodechlorination (HDC) catalysts in the different evolution of their activity during time on stream. Pt/C showed stable activity in the HDC of dichloromethane (DCM) and chloroform (TCM), while Pd/C was deactivated after 90 h of operation, particularly during HDC of DCM. The deactivation of Pd/C catalyst can be attributed to the lower proportion of zero-valent species and larger metal particle size. This appears to hinder the H_2 dissociation, enhance the irreversible chemisorption of reactants and reaction products, and favor coupling reactions (leading to the formation of carbonaceous deposits) and/or metal phase change reactions. The more extensive deactivation of Pd/C in the HDC of DCM is attributed to the stronger chemisorption of the reactant on the catalyst, which leads to the formation of a new PdC_x phase by the incorporation of carbon atoms into the metal lattice.

© 2014 Elsevier B.V. All rights reserved.

1. Introduction

Chloromethanes (CMs) are highly toxic and carcinogenic pollutants [1,2] which contribute to the destruction of the ozone layer, the formation of photochemical smog and global warming [1–3]. Catalytic hydrodechlorination (HDC) is one of the most promising emerging technologies for the abatement of these pollutants since it allows the conversion of organochlorine species into harmless chlorine-free compounds under relatively mild operating conditions, resulting in economic and environmental advantages over other techniques [4–8].

Although HDC of CMs has been investigated to a lesser extent than HDC of other organochlorine compounds, several publications

have appeared in recent years including a number reporting on the deep gas-phase HDC of CMs over different supported metal catalysts [4,5,8–24]. It is well known that precious metals are active catalysts for the hydrogenolysis of the carbon-chlorine bond [8,9]. Among them, palladium has been reported to be a very good option because of its high activity and selectivity to non-chlorinated products [21,25,26]. These studies report on the use of a wide variety of supports including SiO_2 [5,10], Al_2O_3 [11–13], TiO_2 [14–16] and carbon materials [4,17–24]. However, in all cases where the performance as a function of time on stream has been evaluated, Pd catalysts have been shown to suffer severe and rapid deactivation.

In previous studies of our group, the gas-phase HDC of dichloromethane (DCM) and chloroform (TCM) with commercial and laboratory-made activated carbon-supported Pd catalysts (Pd/C) was investigated [4,18–21], with very good results in terms of activity and selectivity to non-chlorinated products. Nevertheless, these catalysts also underwent severe deactivation after a few hours of operation, which is a serious drawback for their potential application. The extent of deactivation was found to be highly dependent on the CM used as the target compound. The most severe deactivation of the Pd/C catalysts was found in the HDC of DCM, the results suggesting that the poisoning of active centers

* Corresponding author at: Ingeniería Química, Facultad de Ciencias, Universidad Autónoma de Madrid, Campus de Cantoblanco, 28049 Madrid, Spain.
Tel.: +34 914976939; fax: +34 914973516.
E-mail addresses: maria.martin.martinez@uam.es (M. Martin-Martinez),
ariadna.alvarez@uam.es (A. Álvarez-Montero), luisa.gomez@uam.es
(L.M. Gómez-Sainero), rtb5@st-andrews.ac.uk (R.T.Baker), pepe.palomar@uam.es
(J. Palomar), salama.omar@uam.es (S. Omar), seser@psu.edu
(S. Eser), juanjo.rodriguez@uam.es (J.J. Rodriguez).

by organochlorine species was the main cause. In contrast to this, Pt/C catalysts, prepared using the same support, were found to be highly stable. In another recent study [22] using monometallic and bimetallic Pd-Pt catalysts with different oxide supports, a bimetallic Pd-Pt catalyst supported on sulfated zirconia also showed a high stability. In both cases the stability of the catalyst was ascribed to the small size of the metallic particles and to the oxidation state of the metals.

The deactivation of metallic catalysts in the HDC of CMs has not been widely investigated and there is no consensus about the causes of deactivation. In gas-phase HDC, deactivation of noble metal catalysts has been linked to poisoning by HCl and/or Cl, formation of carbonaceous deposits, loss of metal through the formation of volatile chlorides, and metal sintering [8,16,23,27–31]. However, most of these studies do not address the HDC of CMs and very few publications refer to activated carbon-supported noble metal catalysts. There is a general agreement on the deactivation of supported metal catalysts by the HCl formed in the HDC of organochlorine compounds. However, the deactivation by HCl is highly dependent on the operating conditions [27], and the nature of the catalysts components. The nature of the support has been reported to have a significant influence on poisoning by HCl [14,32]. Several authors have proposed the formation of carbonaceous deposits, including chlorine in their constitution in many cases, as one of the main causes of deactivation of these catalysts [16,23,28,33,34]. Changes in the oxidation state of Pd have also been reported to play a key role in the deactivation of the catalyst in the HDC of light organochlorine compounds over Pd/TiO$_2$ [16]. The extent of sintering of metal catalysts appears to be related to the nature of the support. Moon et al. [35] reported that the sintering of Pd supported on oxide supports was the main cause of deactivation in the gas-phase hydrodehalogenation of CClF$_2$CF$_3$. On the contrary, other authors observed re-dispersion of metal upon HDC, but when activated carbon was used as the support [20,28,33].

The aim of this work is to conduct an in-depth study on the causes of deactivation of Pd/C catalysts in the HDC of CMs, in the light of the high stability shown by Pt/C catalysts under the same conditions. This would serve to identify the key factors for the design and preparation of highly stable HDC catalysts – a critical issue for the industrial application of this technology. Fresh and used catalysts were characterized by several techniques in order to analyze the possible causes of deactivation. These experimental methods were complemented by a theoretical study of the interactions of DCM with Pd and Pt active species, using quantum-chemical methods in the Density Functional Theory (DFT) framework.

2. Experimental

2.1. Catalysts preparation

Carbon-supported Pd and Pt catalysts were prepared by incipient wetness impregnation of a commercial activated carbon supplied by Erkimia S.A. By chemical analysis, the carbon was found to have a content in heteroatoms of lower than 1 wt.% (S, Fe, Ca, Na, Al, K) and less than 6 wt.% ash content (after heating to 600 °C). Summarizing, the activated carbon had a BET surface area of 1200 m^2 g^{-1}, a micropore volume of 0.62 cm^3 g^{-1} and an external or non-microporous surface area of 0.53 m^2 g^{-1}. The fraction with a particle size of between 0.25 and 0.50 mm was used in this work. Aqueous solutions containing the appropriate amounts of either PdCl$_2$ or H$_2$PtCl$_6$·6H$_2$O (supplied by Sigma–Aldrich) to give a final metal loading of 1 wt%, were added dropwise to the activated carbon while stirring to mix. The volume of aqueous solution used corresponded to the pore volume of the activated carbon.

After drying, activation of the catalysts was carried out by reduction under continuous H$_2$ flow (50 ml min^{-1}). The samples were heated to 250 °C at a rate of 10 °C min^{-1} and maintained at this temperature for 2 h. Hydrogen was supplied by Praxair with a minimum purity of 99.999%.

2.2. Catalyst characterization

The X-Ray Diffraction (XRD) patterns of the catalysts were obtained using an X'Pert PRO Panalytical Diffractometer. The powdered sample was scanned using Cu K$_\alpha$ radiation (λ = 0.15406 nm) using a Ge Mono filter. A scanning range of 2θ from 10° to 100° and a scan step size of 0.020° with 5 s collection time were used.

The surface of the catalysts was analyzed by X-ray photoelectron spectroscopy (XPS) with a Physical Electronics 5700 C Multitechnique System, using Mg Kα radiation ($h\nu$ = 1253.6 eV). To determine all the elements on the catalyst surface, general spectra were recorded for the samples by scanning up to a binding energy of 1200 eV. Partial spectra of C 1s, O 1s, Cl 2p, Pd 3d and Pt 4f were used to determine the chemical state of the elements and their chemical environment on the catalyst surface. Correction for binding energies due to sample charging was done by taking the C 1s peak (284.6 eV) as an internal standard. The accuracy of the binding energy scale was ±0.1 eV. The data analysis procedure involved smoothing, a Shirley background subtraction and curve fitting using mixed Gaussian–Lorentzian functions by a least-squares method. Atomic ratios of the elements were calculated from the relative peak areas of the respective core level lines using Wagner sensitivity factors [36].

Flash Pyrolisis experiments were carried out in a CDS Pyroprobe 1000 coupled to HP 5971 GC/MS. The samples (1 mg) were heated to 480 °C under a continuous He flow at a rate of 5000 °C s^{-1} and maintained at that temperature for 10 s.

Temperature-programmed desorption in flowing He (He-TPD) was carried out in a Micromeritics AutoChem II 2910 instrument connected to a quadrupole mass spectrometer. The samples (0.1 g) were heated to 900 °C at a rate of 10 °C min^{-1}.

Temperature-programmed oxidation (TPO) tests were carried out in a LECO Multi-phase Carbon Analyzer (RC-412 model). The samples (1 mg) were oxidized under continuous O$_2$ flow (750 cm^3 min^{-1}). The experiments were conducted from 110 °C to 1100 °C at 30 °C min^{-1}. The evolved CO$_2$ (including any evolved CO that was oxidized to CO$_2$ on a Cu catalyst positioned after the reactor) was quantified using an IR spectrophotometer.

Scanning Electron Microscopy (SEM) images were obtained in secondary electron (SE) mode to obtain high surface detail and in back-scattered electron (BE) mode to obtain compositional information. The intensity at a point in a BE image is related to the square of the average atomic number at the corresponding point in the sample. This allows phases of different densities to be distinguished. A JEOL JSM 5600 instrument equipped with Energy Dispersive X-ray Spectroscopy (EDS) was used for SE imaging and for recording EDS spectra and compositional maps. A higher resolution JEOL 6700F instrument with Field Emission Gun (FEG) was used for both SE and BE imaging and one additional BE image is presented which was obtained using a JEOL JSM 7800F FEG-SEM instrument. Values of accelerating voltage (in kV) and working distance (WD) are provided in the images. For SEM examination the samples were used as prepared and were not metal- or carbon-coated.

Transmission Electron Microscopy (TEM) images were obtained using a JEOL JEM 2011 instrument operating with a LaB$_6$ filament and at an accelerating voltage of 200 kV and equipped with an EDS unit. The images were captured using a Gatan CCD camera and analyzed using Digital Micrograph 3.4.4 software. This software was also used to apply Fourier transforms to selected regions of the TEM images in order to generate Digital Diffraction Patterns (DDPs).

These can be analyzed in a similar way to true diffraction patterns recorded in the TEM instrument but are more convenient when considering small areas of the sample. The microscope was also used to obtain EDS spectra. For TEM examination the samples were ground and the resulting fine powder was suspended in acetone and deposited onto holey carbon-coated Cu grids.

2.3. Catalytic activity experiments

The activity of the catalysts in the HDC of DCM and TCM was evaluated in a continuous flow reaction system described elsewhere [19], consisting essentially of a 9.5 mm i.d. quartz fixed bed micro-reactor, coupled to a gas chromatograph with a FID detector for the analysis of the reaction products.

The experiments were performed at atmospheric pressure using a total flow rate of 100 N cm^3 min^{-1}, a H$_2$/CM molar ratio of 100, space-time (τ) of 1.7 kg h mol^{-1} and temperature (T) of 250 °C. The gas feed, with a CM concentration of 1000 ppmv, was prepared by mixing the starting CM/N$_2$ commercial mixture and N$_2$ in the appropriate ratios. To check for possible mass transport limitations a series of experiments were performed in which the total flow rate and the catalyst particle size were varied. No significant changes were found within the ranges 0.02–0.06 m s^{-1} gas velocity and 0.25–0.71 mm particle size. Catalyst performance was evaluated in terms of CM dechlorination (mol% of chlorine removed from carbon compounds), CM conversion (X_{DCM}, X_{TCM}) and selectivities to the different reaction products (S_i). Long-term (90 h) experiments were performed to examine the evolution of the catalytic activity as a function of time on stream. The experimental results were reproducible with less than 5% error.

2.4. Computational methods

All computational studies were performed with Gaussian 03 [37] software. The transition metal clusters present a great number of electrons, which reorganize deeply the atomic electron density, so we have simulated palladium and platinum clusters using DFT methods. The B3LYP functional which combines Becke's three parameter nonlocal hybrid exchange potential [38] and the nonlocal correlation functional of Lee, Yang and Parr [39] was used. The chemically inert core orbitals of palladium and platinum clusters were described with the effective core potentials of Hay and Wadt [40], which include relativistic effects on valence electrons, while the external orbitals were represented with a double-ζ basis set using Dunning/Huzinaga full double-ζ basis set (Lanl2DZ), which was also used for the rest of the atoms of the species involved in this study. Thus, all the simulations were conducted at the B3LYP/Lanl2DZ computational level, which has been proved to be reliable for systems involving Pd atoms [41–46]. Full geometry optimization was done for isolated reactants, Pd and Pt clusters and reactants-metal systems. In this work, Pt$_6$ and Pd$_6$ clusters were used as models of reference to simulate the metal active sites of the catalysts, following the criteria developed elsewhere [41]. All structures of Pd and Pt clusters have been optimized for various accessible spin multiple (singlet and triplet) states to determine the most stable structures, associated with the lowest energies. Frequency calculations were performed on the optimized geometries at the same level of theory, to ensure that the systems were at local minima (no imaginary vibration frequencies).

The adsorption energy (E_{ads}) per adsorbed intermediate was defined in terms of the stabilization energy for adsorbate/substrate interactions, calculated according to the expression:

$$E_{ads} = E_{(Metal-adsorbate)} - (E_{Metal} + E_{adsorbate}) \qquad (1)$$

where E_{Metal} and $E_{adsorbate}$ are the electronic energy of isolated Pd$_6$ or Pt$_6$ clusters and the DCM adsorbate, respectively, and
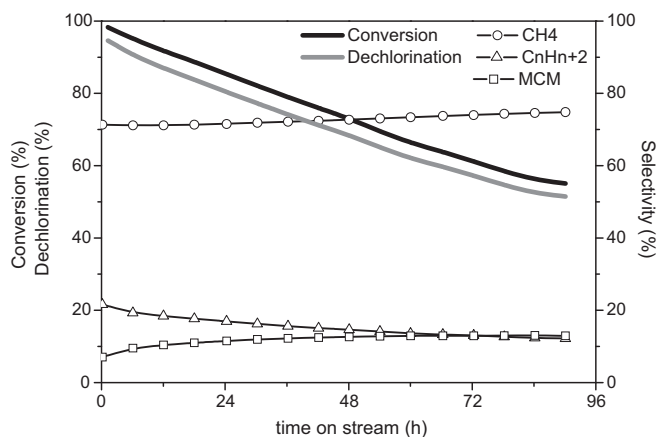

Fig. 1. Evolution of the activity, selectivity to reaction products and overall dechlorination during time on stream in the HDC of DCM with Pd/C.

$E_{Metal-adsorbate}$ is the total energy of the optimized Pd$_6$/Pt$_6$–DCM system. Hence, a positive E_{ads} value indicates an endothermic adsorption process, while a negative one corresponds to an exothermic one. The more negative the E_{ads}, the stronger the adsorption. In addition, the theoretical free energy (G) for each species is predicted at the same computational level including electronic energy (E), zero-point energy, enthalpy temperature corrections (H) and absolute entropy at selected temperatures and 1 atm, derived using the calculated vibrational frequencies and standard statistical thermodynamics relationships. Then, the G and H values of each species involved in adsorption phenomena are used to estimate the Gibbs free energy (ΔG) and the enthalpy (ΔH) of the adsorption by using the expressions:

$$\Delta H = H_{(Metal-adsorbate)} - (H_{Metal} + H_{adsorbate}) \qquad (2)$$

$$\Delta G = G_{(Metal-adsorbate)} - (G_{Metal} + G_{adsorbate}) \qquad (3)$$

3. Results and discussion

3.1. Catalytic activity

Figs. 1 and 2 show the evolution of conversion of DCM and TCM, respectively, during time on stream, when using the Pd/C catalyst. The selectivity to reaction products is also included in both cases. Figs. 3 and 4 show the analogous results for the Pt/C catalyst. As can be observed, both catalysts showed high initial activities but
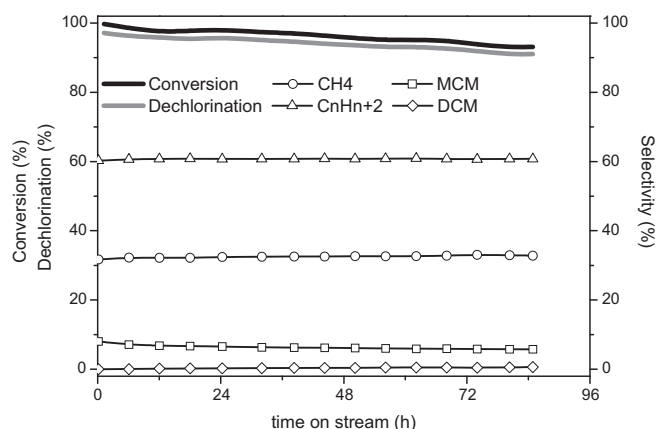

Fig. 2. Evolution of the activity, selectivity to reaction products and overall dechlorination during time on stream in the HDC of TCM with Pd/C.
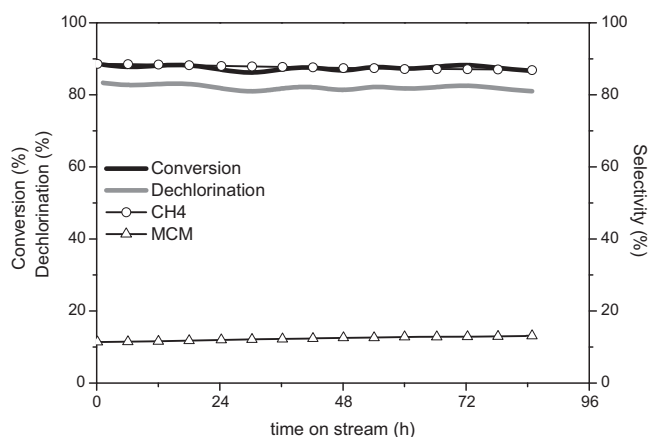
Fig. 3. Evolution of the activity, selectivity to reaction products and overall dechlorination during time on stream in the HDC of DCM with Pt/C.

different stability patterns thereafter, in particular in the HDC of DCM.

The Pt/C catalyst showed high stability, with no loss of activity under either reactant over the 90 h of the experiments. The stability of this catalyst in the HDC of TCM was confirmed previously by an experiment performed at a space time of 0.08 kg h mol^{-1} and a temperature of 200 °C where the catalyst showed stable at a conversion level of 60% [47]. The selectivities to methane (by far the main reaction product) and the other products remained almost constant. Almost complete conversion and dechlorination were achieved in the case of TCM, and values of around 90 and 85%, respectively, with DCM.

However, for Pd/C progressive deactivation was observed under both DCM and TCM, although to different extents. In the HDC of DCM this catalyst showed a rapid and noticeable loss of activity, with similar decreases in DCM conversion and overall dechlorination. Similar results were obtained in a previous study [18] at a lower TCM conversion (space time of 0.24 kg h mol^{-1} and temperature of 150 °C). This suggests that deactivation is mainly associated with a decrease in the number of available active centers. Only small changes in the selectivity patterns are observed. The selectivities to CH_4 and MCM increased somewhat with time on stream at the expense of C_2H_6 and C_3H_8 (represented as C_nH_{n+2}). This suggests some changes in the nature of the active centers. Nevertheless, the changes in selectivity patterns are considerably less pronounced than those in activity.
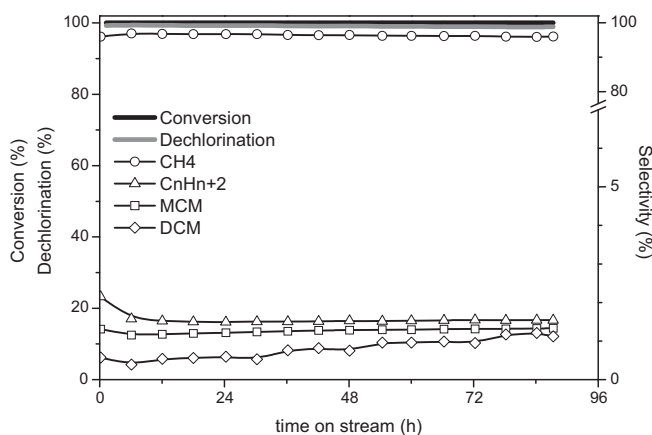

Fig. 4. Evolution of the activity, selectivity to reaction products and overall dechlorination during time on stream in the HDC of TCM with Pt/C.
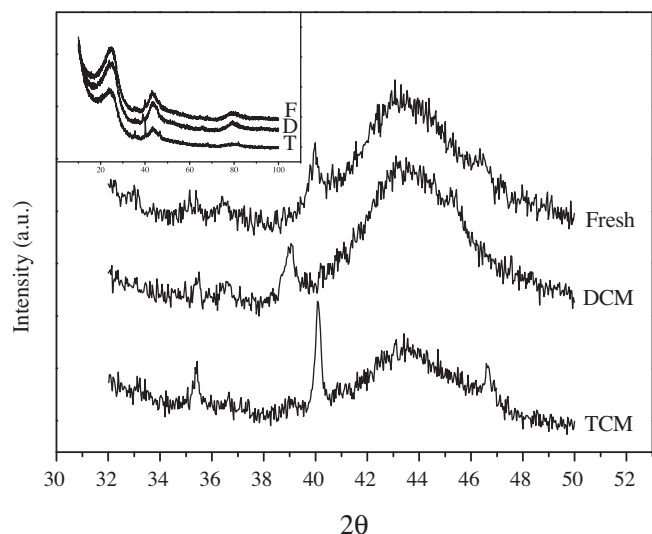

Fig. 5. XRD profiles of the Pd/C catalyst when fresh (F in inset) and after use (90 h on stream in the HDC of DCM (D) or of TCM (T)).

Differences were also found between Pd/C and Pt/C in the HDC of TCM, although these were much less significant than with DCM. Whereas Pt/C remained completely stable over the 90 h on stream of the experiment, a decrease of around 8% in TCM conversion was observed with Pd/C. On the other hand, the selectivity to methane increased slightly to the detriment of the larger hydrocarbons, while the selectivity to CMs decreased slightly.

3.2. Characterization results

3.2.1. Porous structure and metal dispersion

The values of BET surface area, pore volume, and metal dispersion of the Pd/C and Pt/C catalysts, when fresh and after the long-term experiments of Figs. 1–4 have been reported in a previous study [21]. Both catalysts showed a high BET surface area, well above 1000 m^2 g^{-1}, and no significant reduction was observed after the HDC experiments. Thus, constriction or partial blockage of the porous structure did not appear to have occurred at the relatively mild reaction temperature (250 °C) used. CO chemisorption results showed that the fresh catalysts were fairly well and similarly dispersed, with 26% and 24% metal dispersion for Pd/C and Pt/C, respectively. However, in the case of Pd/C, metal dispersion fell to 11% and 12% after 90 h on stream in the HDC of DCM and of TCM, respectively. On the contrary, a significant increase of dispersion was observed for Pt/C, with values of 32% and 34% for the catalysts used with DCM and TCM, respectively. This was attributed to re-dispersion of Pt induced by the reaction environment [20] as will be explained later in the text.

3.2.2. XRD profiles

Fig. 5 shows the XRD profiles of the fresh Pd/C catalyst after reduction and the catalysts after use in HDC. Two peaks corresponding to different Pd-containing phases were observed in all cases, even for the fresh catalyst. That these phases were detected by XRD indicates the presence of relatively large particles. However the fairly high dispersion value obtained indicates that small particles were also present and that the overall size distribution of Pd particles was broad. This was confirmed by TEM (see Section 3.2.5). The line at $2\theta = 35.5°$, present in all the samples, corresponds to palladium chloride. This is consistent with the XPS results where a significant amount of electro-deficient Pd was observed in the fresh catalyst (see later, Fig. 9). As can be seen, this phase does not disappear under the reducing environment of the HDC

experiments which confirms the high stability of electro-deficient Pd species reported in previous studies [8,21]. For the fresh catalyst and that after use with TCM, two peaks corresponding to metallic Pd ($2\theta = 40.2°$ and $46.7°$) were observed. The higher intensity of these peaks after HDC of TCM suggests that some sintering of these metal particles may have occurred. In the catalyst used in the HDC of DCM, these peaks are displaced to lower scattering angles ($2\theta = 39°$ and $45.2°$) than for the fresh catalyst while their intensities remain quite similar. Some authors [48,49] reported similar peaks for palladium black catalysts used for the adsorption of ethene and acetylene at temperatures of 150 °C to 250 °C. Displacement of the Pd metal peaks to a lower scattering angle in used catalysts has also been observed in the hydrodechlorination of CCl_2F_2, $CHClF_2$, and tetrachloroethene [28,50,51]. This shift has been attributed to the formation of palladium carbide (PdC_x). This was reported to involve the deposition of a carbonaceous overlayer followed by an activated diffusion of carbon atoms into the metal lattice. Due to the incorporation of carbon an expansion of the palladium lattice occurs, causing the diffraction peaks to shift to lower scattering angles. A larger shift indicates that more carbon is present in the octahedral holes of the Pd lattice. From calorimetric measurements and theoretical considerations, Ziemecki and Jones [49] calculated that carbon could be incorporated into the Pd structure in sufficient amounts to give carbide stoichiometries up to $PdC_{0.15}$. On the basis of their results, they postulated that the PdC_x phase can be formed by interaction of different carbon-containing molecules with palladium. Ha et al. [51] found that catalyst deactivation occurred because of the formation of palladium carbide. Van de Sandt et al. and Makkee et al. [50,52] concluded that, depending on the reactant used, the outer surface of Pd was clean or covered by an overlayer of carbonaceous deposits. Interstitial carbon did not seem to provoke deactivation of their target reaction but the formation of palladium hydride was hindered and they found changes in the selectivities. Coq et al. [53] also found an expansion of 3% in the interplanar spacing of Pd after hydrogenolysis of CCl_2F_2 over palladium black and palladium/graphite but they suggested that diffusion of chlorine and fluorine into the bulk of palladium was the cause. However, based on the literature, the formation of palladium carbide seems to be a more likely explanation. Malinowski et al. [11], reported carbon incorporation to Pd during HDC of DCM using a **Y**-alumina supported Pd catalyst. The mechanism proposed included the formation of carbene intermediates, some of which, strongly bonded to the active sites, could be further dissociated to give bare carbon atoms. The XRD results presented in Fig. 5 suggest that DCM and TCM interacted differently with the active sites of the catalyst during the respective HDC reactions. This could explain the significant differences observed in the deactivation behavior of the catalyst by exposure to these two reactants.

The XRD patterns of the Pt/C catalysts are shown in Fig. 6. Smaller peaks corresponding to platinum chloride were detected, and no peaks that could be assigned to metallic particles were observed, which is consistent with the high Pt dispersion values of this catalyst and a narrow size distribution of the metallic particles.

3.2.3. TPD, TPO and flash pyrolysis

The fresh and used Pd catalysts where examined by flash pyrolysis GC–MS and He-TPD–MS. Carbon oxides, hexane, benzene and 2-propanone were detected by gas chromatography from pyrolysis of the fresh and used catalyst samples. These compounds must originate from the thermal decomposition of the activated carbon support. In addition, some DCM evolved from the catalyst after use in HDC of DCM, whereas MCM, DCM, TCM and HCl were detected in the catalyst after use in the HDC of TCM. The results are shown in Fig. 7, including the retention times of chlorinated compounds. A wide diversity of hydrocarbons of up to nine carbon atoms were also detected from flash pyrolysis of the catalyst used in the HDC
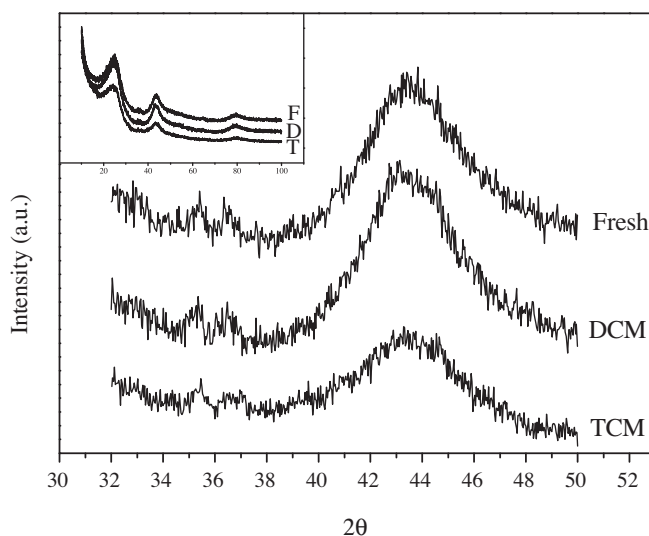

Fig. 6. XRD profiles of the Pt/C catalyst when fresh (F in inset) and after use (90 h on stream in HDC of DCM (D) or of TCM(T)).

of TCM. Fig. 8 shows the DCM, TCM and HCl profiles from TPD/MS of the different samples of Pd/C catalyst. As can be seen, significant amounts of chlorinated compounds were desorbed from the catalyst used in HDC of TCM at temperatures in the range 250–350 °C. The highest intensities were observed for m/z 49 (which shows the maximum of desorption peak at 250 °C) and m/z 36 (with the maximum at 300 °C), indicating that significant poisoning of active sites by DCM and HCl must be taking place during the HDC of TCM. Desorption of TCM was also observed (m/z 83) and also of MCM (m/z 50) although in much lower extent. The higher amount of DCM than TCM chemisorbed on the active centers, despite the higher proportion of the latter in the reaction mixture, is in agreement with the results obtained by molecular simulation [41] where it was found that non-dissociative adsorption of CMs on Pd is thermodynamically favored in the order DCM > MCM > TCM for electro-deficient Pd and MCM > DCM > TCM for zero-valent Pd, the non-dissociative adsorption on electro-deficient Pd being by far the more favored in any case. The TPD profiles of the catalyst used in the HDC of DCM show only a small peak of DCM at a temperature around 300 °C. This suggests a strong interaction of DCM with Pd particles which disfavors its desorption. This is consistent with the results from molecular simulation [41] and XRD, where, as indicated before, the formation of a Pd-C phase was detected in the catalyst used in the HDC of DCM. No HCl desorption was observed in this case, due in part to the lower amount of HCl formed because of the lower chlorine content of the starting molecule and the lower conversion achieved. On the other hand, since HCl and the CMs compete for adsorption on the metallic sites, the high adsorption strength of DCM probably contributes to prevent HCl adsorption. The deposition of hydrocarbons larger than CH_4 in the HDC of TCM is consistent with the higher selectivity to these reaction products than in the HDC of DCM (Figs. 1 and 2) as well as with the larger size of the metallic particles and their concentration in the outer surface of the catalyst, which favor the formation of these compounds. Small particle sizes and homogeneous distribution were found to be key factors in inhibiting the formation of hydrocarbons larger than methane, which cause deactivation of the catalyst [20,22].

TPO experiments showed a loss of carbon within the range of 500–600 °C of 1.6% from the fresh catalyst, whereas it increased up to 3.6% and 11.2% after use in the HDC of DCM and of TCM, respectively. This supports the occurrence of carbon-containing species deposited on the surface of the used catalysts to different extents.
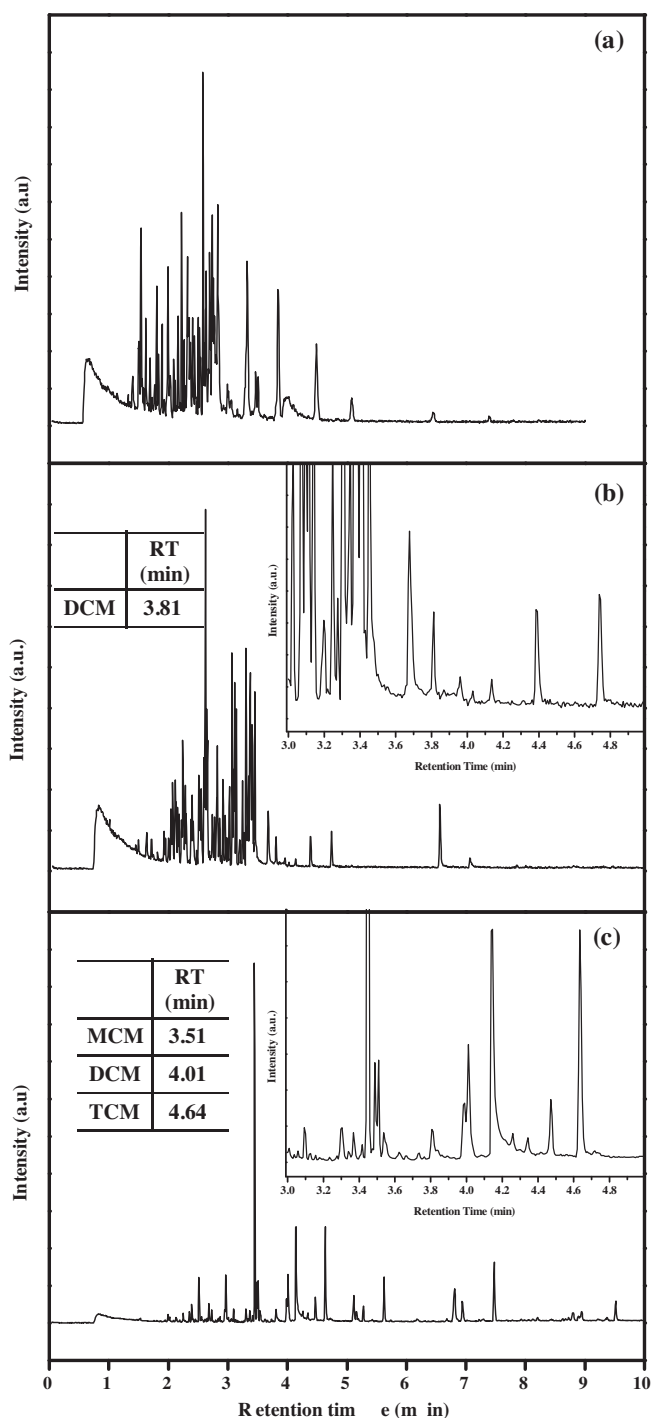
Fig. 7. Flash pyrolisis/GC-MS traces for the Pd/C catalyst when fresh (a) and after usein the HDC of DCM (b) and TCM (c).

3.2.4. XPS results

Fig. 9 shows the XPS profiles of the fresh and used Pd/C catalyst in the Pd 3d region. Two main bands centered at binding energy values around 336 eV and 337.5 eV were observed for Pd $3d_{5/2}$ in all the cases, which can be attributed to metallic (Pd^0) and electro-deficient (Pd^{n+}) palladium, respectively. The formation of electro-deficient species in Pd/C catalysts prepared from H_2PdCl_4, and their presence in the catalysts after being used in the HDC of DCM and TCM has been investigated in previous studies [18,19,54]. As can be seen in the catalyst after its use in the HDC of DCM a new band appears around 336.5 eV which can be attributed to
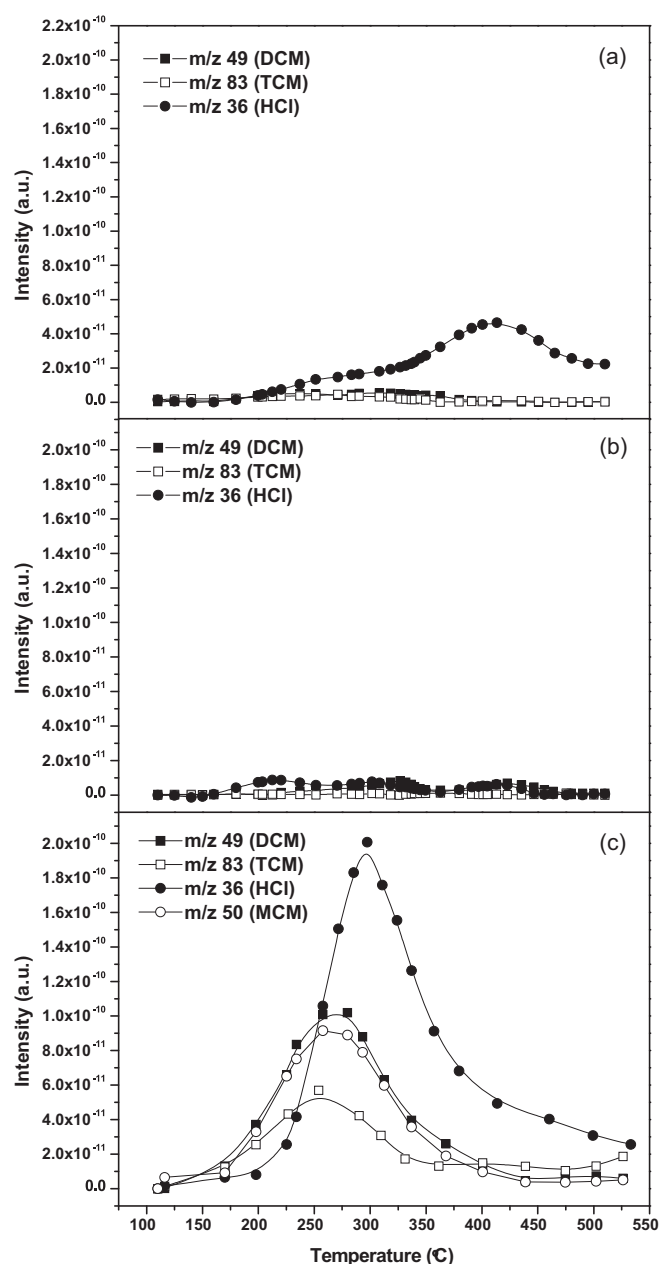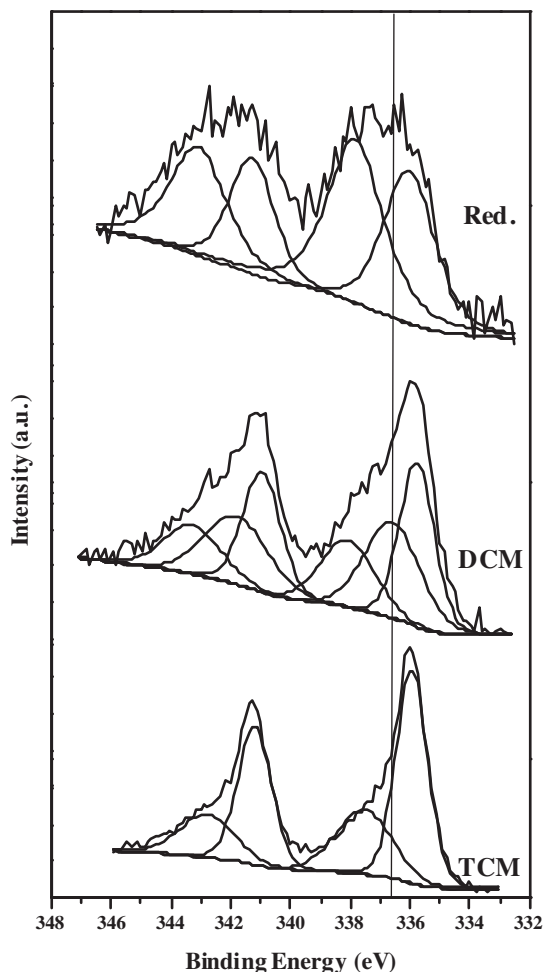

Fig. 8. He-TPD/MS spectra of the Pd/C catalyst when fresh (a) and after use in the HDC of DCM (b) and of TCM (c).
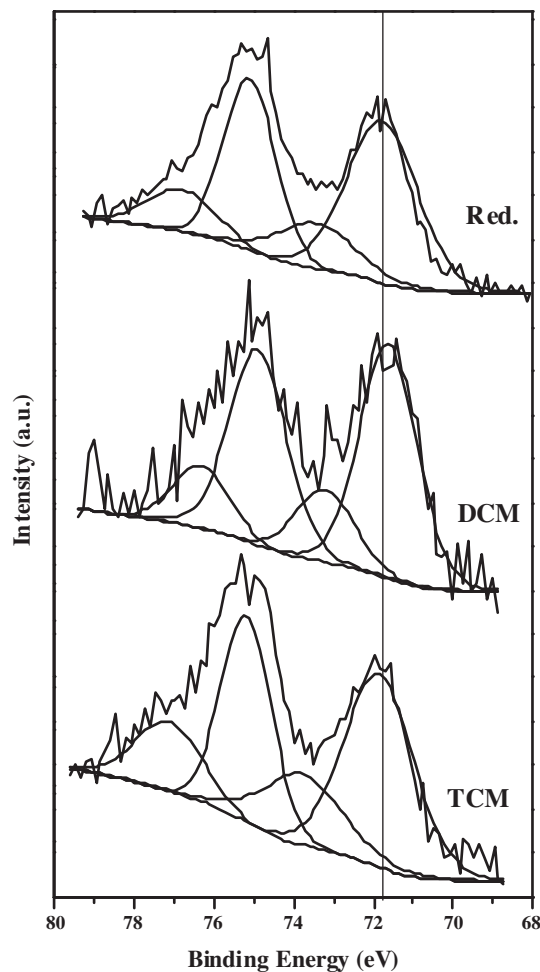
the aforementioned Pd carbide phase (NIST database), indicated in the XRD results. Table 1 summarizes the surface Pd composition (as determined by XPS) and the relative proportions of Pd species at the surface of the fresh and used Pd/C catalyst samples. The surface concentration of chlorine and the relative amount of organic and inorganic chlorine obtained from the deconvolution of the XPS spectra in the Cl_{2p} region are also included. The proportion of Pd present at electrodeficient Pd decreased after HDC. This can be attributed to partial coverage of electrodeficient Pd with the starting chloromethane and/or reaction byproducts since no decrease in the amount of palladium chloride was observed by XRD (Fig. 5). Electro-deficient Pd has been proposed as the main center for molecular chemisorption and formation of hydrocarbons larger than CH_4 [4,18,21]. The proportion of zero-valent Pd also decreased in the HDC of DCM due to the formation of the new PdC_x phase, while an increase was observed for HDC of TCM. It must be noted that whereas the total amount of surface Pd decreased after HDC of

Table 1
XPS results.

Catalyst	M_{XPS} (%)	M_{XPS}/M_{bulk}	M^0 (%)	M^{n+} (%)	PdC_x (%)	Cl_{XPS} (%)	Cl_{inorg} (%)	Cl_{org} (%)
Pd/C	0.17	1.75	4.5	95.5	–	0.35	49.2	50.8
Pd/C reduced	0.32	3.30	52.9	47.1	–	0.11	46.7	53.3
Pd/C used DCM	0.25	2.61	39.1	24.5	36.4	0.13	29.2	70.8
Pd/C used TCM	0.95	9.05	65.7	34.3		1.36	16.0	84.0
Pt/C	0.06	1.15	52.1	47.9	–	0.43	37.6	62.4
Pt/C reduced	0.07	1.34	74.5	25.5	–	0.13	17.0	83.0
Pt/C used DCM	0.04	0.78	68.9	31.1		0.14	18.5	81.5
Pt/C used TCM	0.05	0.98	76.2	23.8		1.44	8.5	91.5

Fig. 9. XPS profiles in the Pd 3d region of the Pd/C catalyst when fresh (a) and after use in HDC of DCM (b) and of TCM (c).

Fig. 10. XPS profiles in the Pt 4f region of the Pt/C when fresh (a) and after use in HDC of DCM (b) and of TCM (c).

DCM, a significant increase was observed after HDC of TCM, which suggests that, in this last case, migration of Pd particles to the outer surface of the catalyst took place. On the other hand, a large increase in surface chlorine occurred after HDC of TCM whereas it remained almost constant after HDC of DCM, which is in agreement with the TPD and pyrolysis results. It seems that migration of Pd is accompanied by the formation of larger particles, as was suggested by the XRD results. Nevertheless, the larger amount of Pd in the outer surface and the higher proportion of zero-valent Pd appear to contribute to the much higher stability of the catalyst in HDC of TCM than in HDC of DCM since there are more active centers accessible to the reactants and more Pd^0 available for H_2 dissociation. This can partially compensate for the loss of active sites caused by their blockage by reactants and products, as indicated by the pyrolysis and TPD results.

Under TCM, more HCl is formed and the reactant is more weakly chemisorbed than under DCM. This may have contributed to the higher mobility of Pd under TCM because of its reaction with HCl, followed by its re-deposition and reduction by the H_2 to form new Pd particles, generally nearer to the surface of the support. Therefore, the results allow us to conclude that the stronger deactivation of the Pd catalyst under DCM can be attributed to the irreversible chemisorption of the reactant and the partial transformation of Pd into a new PdC_x phase by the incorporation into Pd of carbon atoms from the chemisorbed DCM. Solid solutions of Pd could greatly inhibit H_2 dissociation, and the spillover of hydrogen, so decreasing DCM conversion.

Fig. 10 shows the XPS spectra of the fresh and used Pt/C catalyst in the Pt 4f region. The band at a binding energy of 72 eV for Pt $4f_{7/2}$ corresponds to Pt^0 while the value around 73.4 eV corresponds to
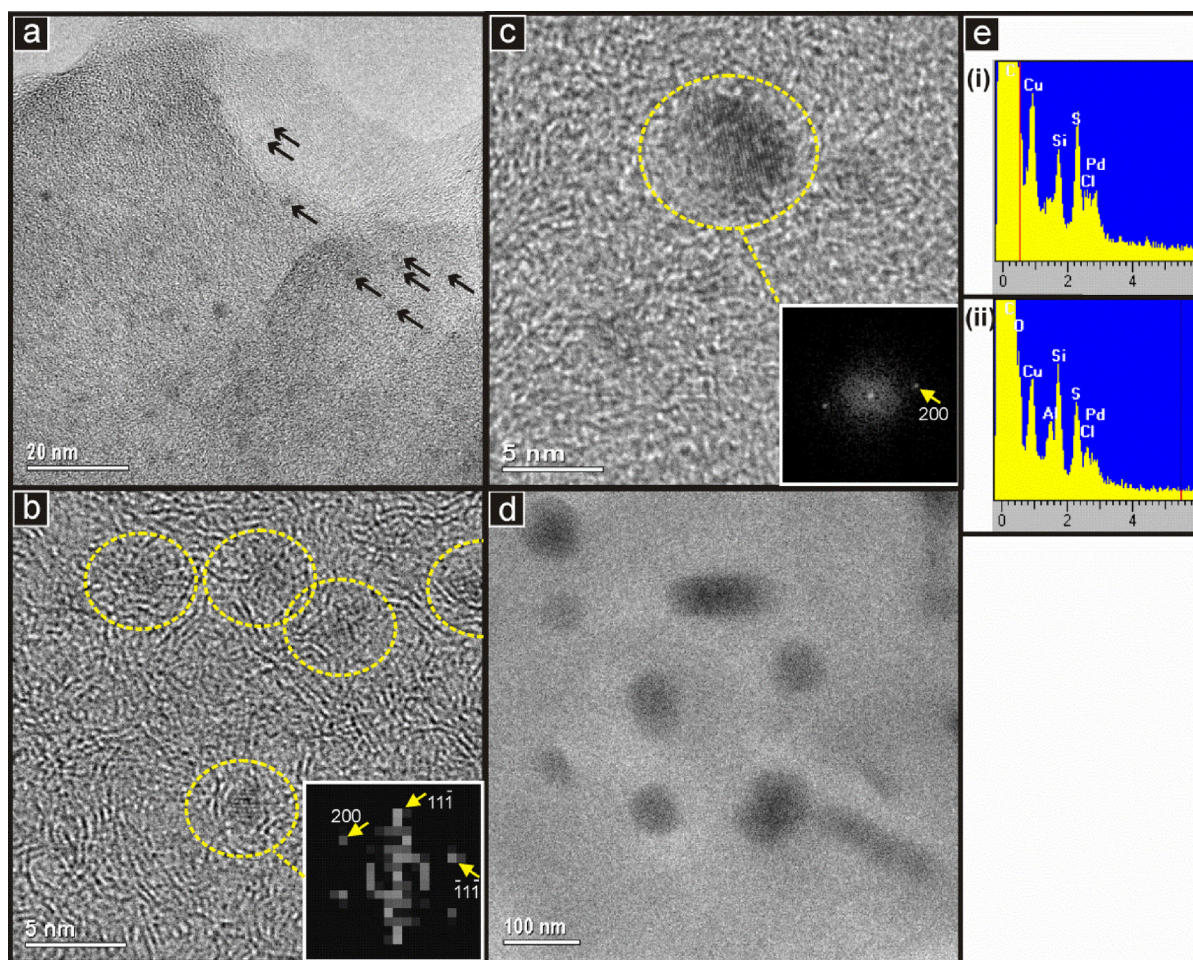
Fig. 11. TEM images of the reduced Pd/C catalyst. See text for details.

Pt^{n+}. The results are summarized in Table 1. As can be seen, the ratio of zero-valent to electrodeficient species is higher than in the Pd catalyst, and the ratio does not change significantly after use in HDC. However, the proportions are not so far from those for Pd/C after use in the HDC of TCM, which showed a much higher stability than with DCM. As shown in Table 1, the surface concentration of platinum remained almost constant after HDC with both reactants and was closer to the bulk concentration than in the case of Pd/C, suggesting than Pt is more homogenously distributed throughout the catalyst. In addition, the absence of XRD peaks corresponding to metallic Pt in any of the three Pt/C samples suggested smaller average Pt particle size than for Pd. The small particle size and homogeneous particle size distribution of Pt was previously confirmed by TEM for the fresh Pt catalysts and those after use with DCM [20]. The smaller proportion of electro-deficient Pt appears to inhibit the non-dissociative adsorption of CMs (see later molecular simulation results in Section 3.3) and the small particle size and homogeneous distribution of Pt on the support [20] prevents the formation and stabilization of hydrocarbons larger than CH_4 (which did occur with Pd/C in TCM HDC) leading to the higher stability of the Pt/C catalyst.

3.2.5. Electron microscopy characterization

TEM images, EDS spectra and DDPs for the Pd/C catalyst both in the fresh state and after use in the HDC of DCM are presented in Figs. 11 and 12, respectively. The three most important Pd-rich phases to consider are metallic Pd, $PdCl_2$ and the Pd-C solid solution (PdC_x) discussed above. Metallic Pd has a cubic *Fm3m* structure with lattice parameter, $a = 3.90$ Å [ICSD code: 41517] and would be

expected to exhibit diffraction spots corresponding to the (2 0 0) and (1 1 1) interplanar spacings, d, of 1.95 and 2.25 Å. It has been reported recently that the form of $PdCl_2$ stable at ambient temperature (designated γ-$PdCl_2$) has a monoclinic ($P12_1/c1$) structure [ICSD code: 421221] and would exhibit diffraction spots at many values of d from 5.3 Å to below the resolving limit of the microscope at about 1.9 Å. The crystal structure of palladium carbide has been determined experimentally only for $PdC_{0.03}$ [ICSD code: 618635]. The structure of this material was the same as for Pd (*Fm3m*) but very slightly expanded, with $a = 3.91$ Å. The XRD data presented above would suggest a more expanded Pd structure – indicating a higher C content – with $d_{200} = 2.01$ Å and $d_{111} = 2.31$ Å, giving $a \approx 4.02$ Å. This represents a linear expansion of only 3% which is difficult to observe in DDPs obtained from TEM images of small particles. Therefore, in such cases, DDPs are indexed to the Pd structure unless there is a significant difference from the corresponding d values.

Fig. 11(a) shows a typical view of the carbon support in the fresh catalyst. A large number of small particles (around 2–5 nm diameter, arrowed) can be seen. Some of these particles are imaged at high magnification in Fig. 11(b) (circled) and the lower of these gave rise to the DDP inset. This DDP is of low resolution because of the very small size of the region of the image used to generate it. Nevertheless, a full diffraction pattern was obtained and this can be indexed to the crystal structure of Pd viewed along the [0 1 1] zone axis. A slightly larger (5 nm) particle with interplanar spacings, d, matching those of the (2 0 0) planes of Pd is shown in Fig. 11(c) and particles of around 30–100 nm – assigned as Pd because of their high contrast and typical morphology – are seen in Fig. 11(d).
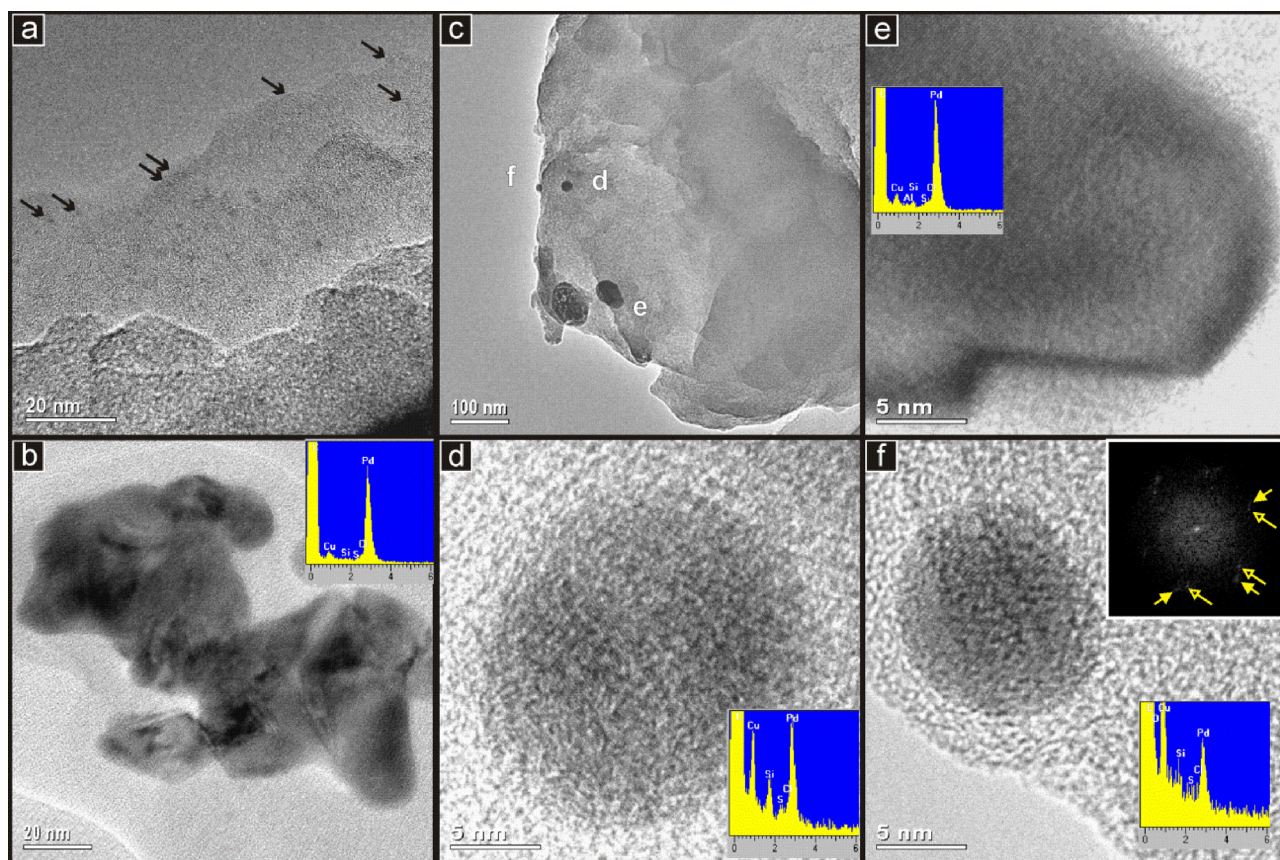
Fig. 12. TEM images of the Pd/C catalyst after use in the HDC of DCM. See text for details.

Avoiding Pd particles larger than 5 nm, EDS spectra were recorded from approximately 100 nm diameter regions of the carbon support in the fresh and used catalyst. These are presented in Fig. 11(e). Relatively small amounts of Pd and Cl were detected in both cases along with significant quantities of Al, S and Si, which are associated with the carbon support itself. The Cu signal is caused by the TEM grids and should be ignored. The very large C signal is offscale.

In the catalyst after use in the HDC of DCM, small particles (2–4 nm) were again observed (Fig. 12(a), arrowed). However, larger particles than this were more commonly found than in the fresh catalyst. A cluster of these larger particles is shown in Fig. 12(b) together with the EDS spectrum which confirmed its composition. Fig. 12(c) shows a general view of a region of the catalyst with some high-contrast particles. High resolution images of three of them are presented in parts (d)–(f), as indicated. The 15 nm particle in part (d) showed interplanar spacings consistent with the (2 0 0) planes of Pd and was confirmed to be Pd by EDS. The largest of the three particles – in part (e) – gave a strong Pd peak in the EDS spectrum and showed d values matching those of the (2 0 0) planes of Pd. The particle in part (f) was also confirmed to be Pd-rich by EDS. It is important that Cl peaks were not observed in the EDS spectra of the Pd-rich particles imaged in Fig. 12(b) and (d–f). This means, of course, that these particles cannot be PdCl$_2$, one of the phases identified by XRD in both the fresh and used Pd/C catalyst. The likely possibilities are then either pure Pd or a palladium carbide.

A DDP was calculated from the whole particle shown in Fig. 12(f) and is included in the figure. The DDP is complex since it contains two sets of spots. The spots in the first set are diffuse, do not seem to form a self-consistent pattern and correspond to d values of 2.06, 2.12 and 2.26 Å (all ±0.05 Å, filled arrows). The observation of two

sets of spots rather than one and the fact that the diffuse spots are not all related to each other, both suggest that the particle is polycrystalline. This may occur through the presence of twin boundaries in a crystallite or through the presence of several crystal phases in the same particle. The spots in the second set are sharper and appear to form a self-consistent pattern (empty arrows in the figure). The three values of d are 2.33, 2.37 and 2.41 Å (all ±0.05 Å) and the spots are arranged at close to 60° to each other. This pattern cannot be explained by the structure of pure Pd and would indicate either a different crystal phase (rich in Pd) or twinning in a single crystallite of Pd. The values of d obtained from both sets of spots are either consistent with or slightly larger than those expected for metallic Pd (1.95 and 2.25 Å). This and the indicated polycrystallinity of the particle suggest that it contained both Pd and the PdC$_x$ phase discussed above, in connection with the XRD results.

FEG-SEM images of the fresh and used Pd/C catalyst are shown in Fig. 13. Both SE images – in which surface structure is well-resolved – and BE images – which provide direct information about the density of the phases in a sample – are given. In the fresh catalyst, large, angular and trapezoidal and smaller more rounded Pd particles were identified by their brightness in BE images (examples arrowed, Fig. 13(a)) and are shown in the SE image in Fig. 13(b). In the higher magnification BE image in part (c) the sub-100 nm particles are seen to have trapezoidal morphologies. Finally, the very high magnification BE image in part (d) provides evidence of Pd particles with diameters down to about 5 nm. These results are consistent with those of TEM, taking into account the different magnification ranges of the two microscopy methods. In the catalyst after use in the HDC of DCM, a new morphology was observed. This is shown in SE images in parts (e) and (f) of Fig. 13. The particles are no longer angular or trapezoidal but rounded, elongated and of more complex shapes. The BE image in part (g) shows the
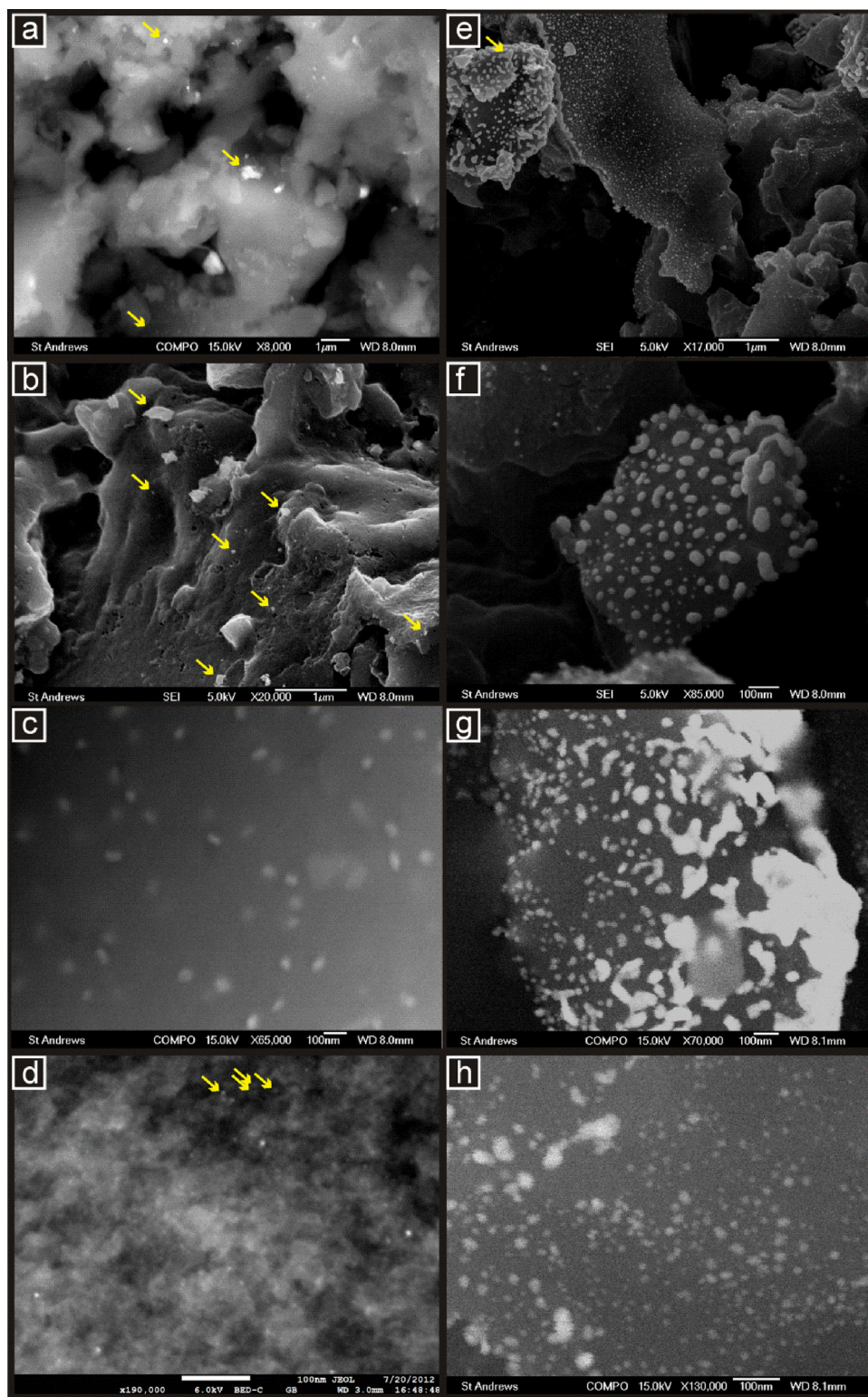
Fig. 13. FEG-SEM images at increasing magnifications of the reduced (a–d) and used (e–f) Pd/C catalysts taken in back-scattered (a, c, d, g, h) and in secondary electron (b, e, f) modes. See text for details.

high brightness of these features, allowing them to be assigned as Pd-rich. These structures were also observed to a certain extent at high magnifications where rounded particles but also irregular structures can be seen (part (h)). This striking change of morphology occurred during the HDC reaction and can be attributed to the formation of a palladium carbide phase, whose existence is supported by the XRD and XPS results. It appears that this phase was formed through the reaction of (chloro)hydocarbon species with Pd.

In the Pt catalyst re-dispersion of metal took place during the HDC reaction [20]. This did not occur with the Pd catalyst and, in fact, agglomeration of Pd particles is indicated. Larger particles appear to favor metallic phase changes (as was the case in the HDC of DCM) and coupling reactions leading to the formation of

Table 2
Calculated thermodynamic parameters (kcal/mol) for DCM adsorption on Pt$_6$ (this work) and Pd$_6$ (from Ref. [43]) clusters calculated at B3LYP/Lanl2DZ computational level.

kcal/mol	Metal species			Dissociative adsorption			Non dissociative adsorption		
	E_{ads}	ΔH	ΔG	E_{ads}	ΔH	ΔG	E_{ads}	ΔH	ΔG
Pt$_6^0$(Singlet)	19.2	19.2	20.5	−60.6	−60.7	−48.5	10.0	11.0	19.2
Pt$_6^0$(Triplet)	–	–	–	−69.3	−69.7	−59.1	−12.3	−11.6	−0.98
Pt$_6^{2+}$(Singlet)	17.1	17.1	14.9	−33.1	−33.1	−24.1	−37.4	−28.4	−26.6
Pt$_6^{2+}$(Triplet)	–	–	–	−56.4	−56.4	−46.0	−46.2	−45.1	−36.5
Pd$_6^0$(Singlet)	7.0	7.0	10.1	−46.8	−47.5	−34.8	1.6	2.7	11.1
Pd$_6^0$(Triplet)	–	–	–	−60.1	−60.7	−48.6	−5.9	−4.8	1.2
Pd$_6^{2+}$(Singlet)	13.4	13.3	11.8	−44.7	−45.6	−37.3	−21.9	−20.9	−12.4
Pd$_6^{2+}$(Triplet)	–	–	–	−51.9	−52.5	−43.2	−48.6	−47.5	−38.6

carbonaceous deposits (as was observed in the pyrolysis experiments performed on the catalyst used in the HDC of TCM). The resistance of Pd particles to re-dispersion can be related to their stronger interaction with the support.

3.3. Molecular simulation

DFT calculations have been performed to study the interaction of DCM with *Pd*-based and *Pt*-based catalysts. The molecular model used to simulate the metallic active species consists of subnanometer Pt$_6$ and Pd$_6$ clusters, representing a catalyst with extremely dispersed particles (then neglecting the possible influence of the support on the activity). Despite this simplification, some relevant information has been gained relative to the elementary processes that occur when gaseous DCM molecules interact with surface Pt and Pd species. Table 2 collects the adsorption energy (E_{ads}), enthalpy (ΔH) and Gibbs free energy (ΔG) of adsorption, calculated at the B3LYP/Lanl2DZ level, for the reaction pathway describing the activation of DCM over a *Pt$_6$* surface. These values are compared with those reported for Pd$_6$ [41]. The possible presence of both zero-valent and electro-deficient metallic species in the catalysts was considered.

Firstly, regarding the computational analysis of independent metal species, we observed that a zero-valent Pt triplet structure, Pt$_6^0$, was significantly more stable than that presenting the singlet state, as was also found [43] for the Pd$_6^0$ cluster (Table 2). Both singlet and triplet Pd$_6^0$ structures present similar bond-distances and symmetry and negligible dipole moments, indicating spherical charge distribution for the simulated catalytic particles of Pt, as was found for Pd species [41].

As shown in Table 2, theoretical calculations confirm that both dissociative and non-dissociative adsorption of DCM on the Pt surface is strongly favored, as was previously found for DCM adsorption on Pd active sites. In fact, dissociated DCM-Pt and DCM-Pd complexes may be formed with both zero-valent and electro-deficient Pt and Pd clusters in the triplet state, with high adsorption enthalpies (<−50 kcal/mol) and without activation barriers. The dissociative adsorption of DCM on Pd or Pt active sites occurs via the scission of C–Cl bonds, promoted by the formation of C-Pd/Pt linkages. This suggests the possibility of considering the direct formation of carbene (CH$_2$**) intermediate during HDC process, in agreement with the reaction scheme previously proposed from experimental studies [41]. On the other hand, theoretical results show that DCM can be also adsorbed without intramolecular bond breakages on both zero-valent and electro-deficient Pd and Pt surfaces in the triplet state. However, it is noticeable that the non-dissociative adsorption of DCM over electro-deficient species is remarkably favored in energy for both metals. The values of adsorption enthalpies (<−45 kcal/mol) for the most stable

triplet state correspond to irreversible chemical adsorption (equilibrium constants >10^{33} estimated at 298 K from values in Table 2, ΔG < −35 kcal/mol) and are one order of magnitude higher than the values for non-dissociative adsorption of DCM on zero-valent clusters, which can be classified as physical adsorption. Therefore, it is expected a high concentration of DCM-Pd and H$_2$C-Pd$_2$ species onto the Pd/AC catalyst surface due to its high proportion of electro-deficient Pd species. The presence of the thermodynamically favored CH$_2$** species adsorbed on metal surface may promote the formation of C–C bond, and eventually, the formation of carbonaceous deposits. On the other hand, the presence of DCM molecules chemically adsorbed onto electro-deficient Pd species implied the poisoning of these active centers. These results support the conclusion of Pd/C poisoning by chloromethanes derived from thermal and XPS analyses and the greater deactivation of this catalyst compared to Pt/C.

4. Conclusions

The stability of Pd/C and Pt/C catalysts in the HDC of CMs strongly depends on the metal and the reactant involved. No loss of activity was found for Pt/C when it was used with both DCM and TCM. In contrast, significant deactivation was observed for Pd/C in the HDC of DCM during time on stream (the decrease in conversion was higher than 40% after 90 h), though it was considerably less noticeable in the HDC of TCM (8% decrease in conversion after 90 h). The more severe deactivation of Pd/C can be attributed to the larger average metal particle size and the smaller proportion of Pd in the zero-valent state. In contrast to the small metal particles with a homogeneous size distribution found in Pt/C catalysts after the reaction, much larger metal particles were evident in the Pd/C catalysts through XRD and TEM examination. It appears that Pd/C catalysts favor coupling reactions leading to the formation of carbonaceous deposits and/or changes in metal phase during HDC. On the other hand, the larger proportion of electro-deficient Pd species in the Pd/C catalyst favors the irreversible chemisorption of choloromethanes as indicated by DFT molecular simulation calculations. Moreover, the stronger chemisorption of DCM when compared to TCM, may lead to a stronger deactivation of Pd/C with the former, which is enhanced by the formation of a new PdC$_x$ phase upon the incorporation in the Pd lattice of carbon atoms from the DCM.

were performed at the Electron Microscopy Facility at the University of St Andrews. We are grateful to JEOL UK Ltd for the provision of an additional high resolution image (Fig. 13(d)).

References

[1] E.D. Goldberg, Sci. Total Environ. 100 (1991) 17–28.
[2] M. Tancrede, R. Wilson, L. Zeise, E.A.C. Crouch, Atmos. Environ. 21 (1987) 21872205.
[3] W.J. Hayes, E.R. Laws, Handbook of Pesticide Toxicology, Academic Press, San Diego, 1991.
[4] M.A. Alvarez-Montero, L.M. Gómez-Sainero, J. Juan-Juan, A. Linares-Solano, J.J. Rodriguez, Chem. Eng. J. 162 (2010) 599–608.
[5] S. Ordonez, H. Sastre, F.V. Diez, Appl. Catal. B 25 (2000) 49–58.
[6] M. Legawiec-Jarzyna, A. Srebowata, W. Juszczyk, Z. Karpinski, React. Kinet. Catal. Lett. 87 (2006) 291–296.
[7] H.M. Chiang, J.W. Bozzelli, Combust. Fundam. Appl. Jt. Tech. Meet. Cent. East. States Sect. Combust. Inst., 1993, pp. 322–324.
[8] F.J. Urbano, J.M. Marinas, J. Mol. Catal. A 173 (2001) 329–345.
[9] V.I. Kovalchuk, J.L. d'Itri, Appl. Catal. A 271 (2004) 13–25.
[10] T. Mori, K. Hirose, T. Kikuchi, J. Kubo, Y. Morikawa, J. Jpn. Pet. Inst. 45 (2002) 256–259.
[11] A. Malinowski, D. Lomot, Z. Karpinski, Appl. Catal. B 19 (1998) 79–86.
[12] E. Lopez, S. Ordonez, H. Sastre, F.V. Diez, J. Hazard. Mater. 97 (2003) 281–294.
[13] E. Lopez, S. Ordonez, F.V. Diez, Appl. Catal. B 62 (2006) 57–65.
[14] B. Aristizabal, C.A. Gonzalez, I. Barrio, M. Montes, C.M. de Correa, J. Mol. Catal. A 222 (2004) 189–198.
[15] C.A. Gonzalez Sanchez, C.O. Maya Patino, C.M. de Correa, Catal. Today 133 (2008) 520–525.
[16] C.A. Gonzalez, M. Bartoszek, A. Martin, C.M. de Correa, Ind. Eng. Chem. Res. 48 (2009) 2826–2835.
[17] L. Prati, M. Rossi, Appl. Catal. B 23 (1999) 135–142.
[18] M.A. Álvarez-Montero, L.M. Gómez-Sainero, M. Martin-Martinez, F. Heras, J.J. Rodriguez, Appl. Catal. B 96 (2010) 148–156.
[19] Z.M. de Pedro, L.M. Gomez-Sainero, E. Gonzalez-Serrano, J.J. Rodriguez, Ind. Eng. Chem. Res. 45 (2006) 7760–7766.
[20] M.A. Alvarez-Montero, L.M. Gomez-Sainero, A. Mayoral, I. Diaz, R.T. Baker, J.J. Rodriguez, J. Catal. 279 (2011) 389–396.
[21] M. Martin-Martinez, L.M. Gómez-Sainero, M.A. Álvarez-Montero, J. Bedia, J.J. Rodriguez, Appl. Catal. B 132–133 (2013) 256–265.
[22] J. Bedia, L.M. Gómez-Sainero, J.M. Grau, M. Busto, M. Martin-Martinez, J.J. Rodriguez, J. Catal. 294 (2012) 207–215.
[23] W.D. Rhodes, V.I. Kovalchuk, Mark A. McDonald, Catal. Commun. 18 (2012) 98–101.
[24] S. Ordóñez, E. Díaz, R.F. Bueres, E. Asedegbega-Nieto, H. Sastre, J. Catal. 272 (2010) 158–168.
[25] M. Makkee, A. Wiersma, E.J.A.X. van de Sandt, H. van Bekkum, J.A. Moulijn, Catal. Today 55 (2000) 125–137.
[26] A. Wiersma, E.J.A.X. van de Sandt, M.A. den Hollander, H. van Bekkum, M. Makkee, J.A. Moulijn, J. Catal. 177 (1998) 29–39.
[27] P. Forni, L. Prati, M. Rossi, Appl. Catal. B 14 (1997) 49–53.
[28] S. Ordonez, F.V. Diez, H. Sastre, Appl. Catal. B 31 (2001) 113–122.
[29] B. Heinrichs, F. Noville, J. Schoebrechts, J. Pirard, J. Catal. 220 (2003) 215–225.
[30] D. Chakraborty, P.P. Kulkarni, V.I. Kovalchuk, J.L. d'Itri, Catal. Today 88 (2004) 169–181.
[31] M. Legawiec-Jarzyna, A. Srebowata, W. Juszczyk, Z. Karpinski, J. Mol. Catal. A 224 (2004) 171–177.
[32] G. Yuan, C. Louis, L. Delannoy, M.A. Keane, J. Catal. 247 (2007) 101–256.
[33] T. Mori, T. Yasuoka, Y. Morikawa, Catal. Today 88 (2004) 111–120.
[34] N.C. Concibido, T. Okuda, W. Nishijima, M. Okada, Appl. Catal. B 71 (2007) 64–69.
[35] D. Ju Moon, M. Jo Chung, K. You Park, S. In Hong, Appl. Catal. A 168 (1998) 159–170.
[36] C.D. Wagner, L.E. Davis, M.V. Zeller, J.A. Taylor, R.H. Raymond, L.H. Gale, Surf. Interface Anal. 3 (1981) 211–225.
[37] M.J. Frisch, G.W. Trucks, H.B. Schlegel, G.E. Scuseria, J.R.C.M.A. Robb, J.A. Montgomery Jr., T. Vreven, K.N. Kudin, J.C. Burant, J.M. Millam, S.S. Iyengar, J. Tomasi, V. Barone, B. Mennucci, M. Cossi, G. Scalmani, N. Rega, G.A. Petersson, H. Nakatsuji, M. Hada, M. Ehara, K. Toyota, R. Fukuda, J. Hasegawa, M. Ishida, T. Nakajima, Y. Honda, O. Kitao, M.K.H. Nakai, X. Li, J.E. Knox, H.P. Hratchian, J.B. Cross, V. Bakken, C. Adamo, J. Jaramillo, R. Gomperts, R.E. Stratmann, O. Yazyev, A.J. Austin, R. Cammi, C. Pomelli, J.W. Ochterski, P.Y. Ayala, K. Morokuma, G.A. Voth, P. Salvador, J.J. Dannenberg, V.G. Zakrzewski, S. Dapprich, A.D. Daniels, M.C. Strain, D.K.M.O. Farkas, A.D. Rabuck, K. Raghavachari, J.B. Foresman, J.V. Ortiz, Q. Cui, A.G. Baboul, S. Clifford, J. Cioslowski, B.B. Stefanov, G. Liu, A. Liashenko, P. Piskorz, I. Komaromi, R.L. Martin, D.J. Fox, T. Keith, M.A. Al-Laham, C.Y. Peng, A. Nanayakkara, M. Challacombe, P.M.W. Gill, B. Johnson, W. Chen, M.W. Wong, C. Gonzalez, J.A. Pople, Gaussian 03, Revision E.01, Inc., Wallingford, CT, 2004.
[38] A.D. Becke, J. Chem. Phys. 98 (1993) 5648–5652.
[39] C.T. Lee, W.T. Yang, R.G. Parr, Phys. Rev. B 37 (1988) 785–789.
[40] P.J. Hay, W.R. Wadt, J. Chem. Phys. 82 (1985) 270–283.
[41] S. Omar, J. Palomar, L.M. Gomez-Sainero, M.A. Alvarez-Montero, M. Martin-Martinez, J.J. Rodriguez, J. Phys. Chem. C 115 (2011) 14180–14192.
[42] J. Moc, D.G. Musaev, K. Morokuma, J. Phys. Chem. A 107 (2003) 4929–4939.
[43] Y. Wang, Z. Cao, Q. Zhang, Chem. Phys. Lett. 376 (2003) 96–102.
[44] N. Meiyan, Z. Zeng, J. Mol. Struct. Theochem. 910 (2009) 14–19.
[45] G. Barone, D. Duca, F. Ferrante, G. La Manna, Int. J. Quantum Chem. 110 (2010) 558–562.
[46] E.D. German, I. Efremenko, M. Sheintuch, J. Phys. Chem. A 105 (2001) 11312–11326.
[47] M.A. Alvarez-Montero, Hidrodecloración catalítica de clorometanos en fase gas mediante catalizadores metálicos soportados sobre carbón activo, in: PhD Thesis, Universidad Autónoma de Madrid, Madrid, 2012.
[48] S.B. Ziemecki, D.G. Schwarzfager, G.A. Jones, J. Am. Chem. Soc. 107 (1985) 4547–4548.
[49] S.B. Ziemecki, G.A. Jones, J. Catal. 95 (1985) 621–622.
[50] E.J.A.X. Van de Sandt, A. Wiersma, M. Makkee, H. van Bekkum, J.A. Moulijn, Appl. Catal. A 155 (1997) 59–73.
[51] J.M. Ha, D. Kim, J. Kim, S.K. Kim, B.S. Ahn, J.W. Kang, Chem. Eng. J. 213 (2012) 346–355.
[52] M. Makkee, E.J.A.X. Van de Sandt, A. Wiersma, J.A. Moulijn, J. Mol. Catal. A: Chem. 134 (1998) 191–200.
[53] B. Coq, J.M. Cognion, F. Figueras, D. Tournigant, J. Catal. 141 (1993) 21–33.
[54] L.M. Gomez-Sainero, X.L. Seoane, J.L.G. Fierro, A. Arcoya, J. Catal. 209 (2002) 279–288.